Frontiers of Information Technology & Electronic Engineering
www.jzus.zju.edu.cn; engineering.cae.cn; www.springerlink.com
ISSN 2095-9184 (print); ISSN 2095-9230 (online)
E-mail: jzus@zju.edu.cn

Dot-shaped beamforming analysis of subarray-based sin-FDA*

Bo WANG[†‡1], Jun-wei XIE[1], Jing ZHANG[2], Jia-ang GE[1]

[1]*Air and Missile Defense College, Air Force Engineering University, Xi'an 710051, China*

[2]*Shaanxi Vocational and Technical College of Transport, Xi'an 710018, China*

[†]E-mail: wb_wangbo1991@163.com

Received Nov. 14, 2018; Revision accepted June 23, 2019; Crosschecked Oct. 10, 2019

Abstract: Phased array (PA) radar is one of the most popular types of radar. In contrast to PA, the frequency diverse array (FDA) is a potential solution to suppress range-related interference because of its time-range-angle-dependent beampattern. However, the range-angle coupling inherent in the FDA transmit beampattern may degrade the output signal-to-interference-plus-noise ratio (SINR). We propose a dot-shaped beamforming method based on the analyzed four subarray-based FDAs and subarray-based planar FDAs using a sinusoidally increasing frequency offset with elements transmitting at multiple frequencies. The numerical results show that the proposed approach outperforms the existing log-FDA with logarithmical frequency offset in transmit energy focus, sidelobe suppression, and array resolution. Comparative simulation results validate the effectiveness of the proposed method.

Key words: Frequency diverse array; Subarray-based frequency diverse array; Decoupling; Dot-shaped beamforming
https://doi.org/10.1631/FITEE.1800722 **CLC number:** TN973.21

1 Introduction

Phased array antennas have been widely used for several decades in civil and military applications to improve signal processing performance (Fenn, 2008; Hansen, 2009; Keizer, 2011). However, the range-dependent interference cannot be directly suppressed by beamforming without multiple antennas or a multibeam antenna based on a phased array (PA). The frequency diverse array was initially designed to form a range-dependent beampattern (Antonik et al., 2006a; Wicks and Antonik, 2008, 2009). In contrast to the PA, the frequency diverse array (FDA) employs a tiny frequency increment relative to the carrier frequency across the antenna elements, resulting in a range-angle-dependent beampattern (Antonik et al., 2006b; Wang et al., 2012; Basit et al., 2015; Xu et al., 2015). Due to the additional controllable degrees of freedom of the array, FDA has sparked many interesting investigations (Baizert et al., 2006; Shin et al., 2013; Cetintepe and Demir, 2014; Hu et al., 2017; Zhang et al., 2017).

However, the range and angle of the FDA cannot be exclusively determined at the output of the array because of the range-angle-coupled transmit beampattern. To eliminate the inherent range-angle-coupled relationship, useful achievements have been obtained, which can be divided into two categories. One category is based on the design of the frequency increment or transmit weight (Khan et al., 2014, 2015, 2016a, 2016b; Wang et al., 2016; Basit et al., 2017; Li et al., 2017). Another category is based on the design of the array configuration (Jones and Rigling, 2012; Sammartino et al., 2013; Wang WQ, 2014; Wang and So, 2014; Wang WQ et al., 2014; Xu et al., 2017; Wang SL et al., 2018). In fact, the best decoupling approach is to form a dot-shaped beampattern rather than an S-shaped beampattern, which generates the maxima at multiple ranges and angle values (Liu, 2016; Shao et al., 2016).

‡ Corresponding author

* Project supported by the National Natural Science Foundation of China (No. 61503408)

ORCID: Bo WANG, http://orcid.org/0000-0003-1434-0391

The essence of subarray-based FDA (SB-FDA) is to divide the uniform linear array FDA (ULA-FDA) into multiple subarrays, which employ the same or distinct frequency increments. In this study, we propose a cross SB-FDA to achieve the dot-shaped transmit beampattern. It is difficult to obtain the desired results based only on the design of the array configuration. Therefore, we introduce a sinusoidally increasing frequency offset into the FDAs and planar FDAs, which transmit multiple frequencies to achieve the dot-shaped beam steering to the desired range and angle pair.

2 Data model

2.1 Uniform linear array FDA

The configuration of the basic ULA-FDA is shown in Fig. 1. The frequency radiated from the n^{th} element is expressed as

$$f_n = f_0 + n\Delta f, \quad n = 0,\ 1,\ \ldots,\ N-1, \tag{1}$$

where f_0 is the carrier frequency (also the radiation frequency of the reference element), Δf the frequency offset, and N the number of antenna elements. Under the narrowband assumption, the monochromatic continuous signal transmitted by the n^{th} element can be given as

$$s_n(t) = \exp\left(\mathrm{j}2\pi f_n t\right),\ n = 0,\ 1,\ \ldots,\ N-1. \tag{2}$$

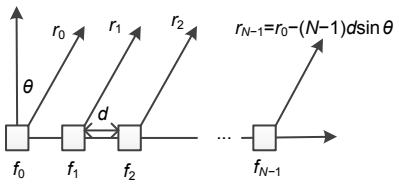

Fig. 1 Basic uniform linear array frequency diverse array (ULA-FDA)

The signal received by a specific far-field location with an angle θ and a slant range R for the first element is a superposition of the delayed and attenuated version of the transmitted signal, expressed as

$$s_n\left(t-\frac{r_n}{c}\right) = \exp\left[\mathrm{j}2\pi f_n\left(t-\frac{r_n}{c}\right)\right], \tag{3}$$

where $r_n = R - nd\sin\theta$ is the range of the target from the n^{th} antenna element, d denotes the element spacing, and c is the speed of light. Hence, the total electric field (E_{T}) observed at the far-field point (R, θ) is computed as

$$\begin{aligned} E_{\mathrm{T}} &= \sum_{n=0}^{N-1}\frac{1}{R}f_{\mathrm{e}}(\omega_0+n\Delta\omega)\cdot\exp\left[\mathrm{j}2\pi f_n\left(t-\frac{R}{c}+\frac{nd\sin\theta}{c}\right)\right] \\ &= \sum_{n=0}^{N-1}\frac{1}{R}f_{\mathrm{e}}(\omega_0+n\Delta\omega)\exp\left[\mathrm{j}2\pi f_0\left(t-\frac{R}{c}\right)\right. \\ &\quad \left.+\,2\mathrm{j}\pi n\left(\Delta f t+\frac{f_0 d\sin\theta}{c}-\frac{\Delta f R}{c}+\frac{n\Delta f d\sin\theta}{c}\right)\right], \end{aligned} \tag{4}$$

where f_{e} represents the directional function of the element. Considering that a target locates at (R, θ), the steering vector $\boldsymbol{a}(R,\theta)$ can be expressed as

$$\boldsymbol{a}(R,\theta) = \left[1, \mathrm{e}^{-\mathrm{j}\left(\frac{2\pi f_0 d\sin\theta}{c}+\frac{2\pi\Delta f d\sin\theta}{c}-\frac{2\pi R\Delta f}{c}\right)}, \ldots, \mathrm{e}^{-\mathrm{j}\left(\frac{2\pi f_0(N-1)^2 d\sin\theta}{c}+\frac{2\pi\Delta f(N-1)^2 d\sin\theta}{c}-\frac{2\pi R(N-1)^2\Delta f}{c}\right)}\right]^{\mathrm{H}}. \tag{5}$$

According to Eq. (5), $2\pi(N-1)^2\Delta f\cdot d\sin\theta/c$ can be approximated as a function of the number of array elements, expressed as $\psi = 2\pi(N-1)^2\cdot\Delta f d\sin\theta/c$ (Fig. 2). Fig. 2 shows that if the number of array elements is no more than 60, then ψ will be smaller than $\pi/4$, implying that the approximation errors are ignorable.

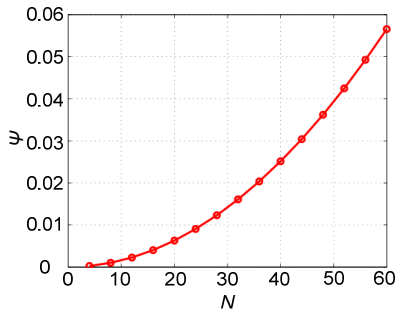

Fig. 2 Ψ changes as a function of the number of array elements

Considering the assumption that $f_{\mathrm{e}}(\omega_0+n\Delta\omega)\approx f_{\mathrm{e}}(\omega_0)$, which denotes the array directional function, Eq. (4) can be rewritten as

$$E_{\mathrm{T}}=\frac{f_{\mathrm{e}}(\omega_0)}{R}\exp\left[\mathrm{j}2\pi f_0\left(t-\frac{R}{c}\right)\right]\cdot\sum_{n=0}^{N-1}\exp\left[\mathrm{j}2\pi n\left(\Delta f t+\frac{f_0 d\sin\theta}{c}-\frac{\Delta f R}{c}\right)\right]. \tag{6}$$

The array factor (AF) at the target position (R, θ) can be derived as

$$\begin{aligned}\mathrm{AF}(t;R,\theta)&=\sum_{n=0}^{N-1}\frac{1}{r_n}\exp\left[\mathrm{j}2\pi f_n\left(t-\frac{R}{c}+\frac{nd\sin\theta}{c}\right)\right]\\&\approx\frac{\exp(\mathrm{j}\phi_0)}{R}\cdot\frac{\sin\left[N\pi\left(\Delta f t-\frac{\Delta f R}{c}+\frac{df_0\sin\theta}{c}\right)\right]}{\sin\left[\pi\left(\Delta f t-\frac{\Delta f R}{c}+\frac{df_0\sin\theta}{c}\right)\right]},\end{aligned} \tag{7}$$

where $\phi_0=2\pi f(t-R/c)-\pi(N-1)(\Delta f t-df_0\sin\theta+\Delta f R)$.

Fig. 3 shows the transmit beampattern of the basic FDA using the simulation parameters listed in Table 1.

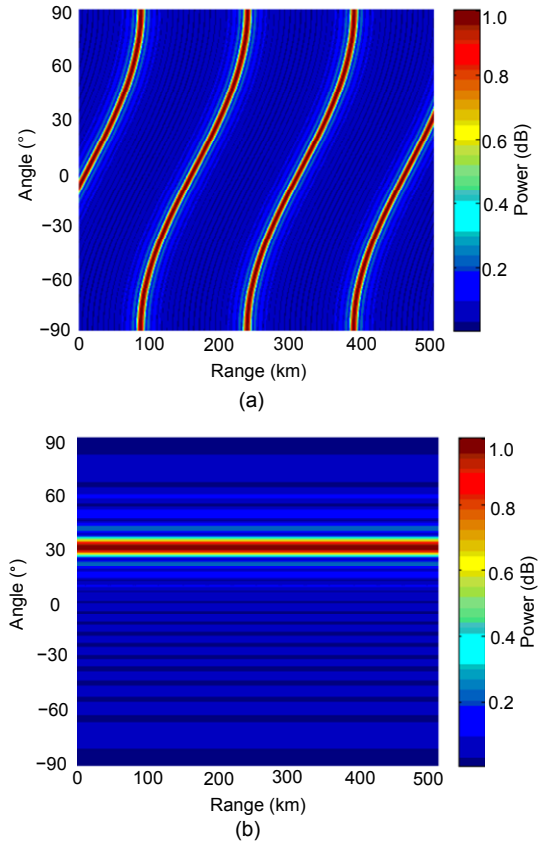

Fig. 3 Transmit beampattern based on a one-dimensional array structure: (a) ULA-FDA transmit beampattern; (b) PA transmit beampattern

Table 1 Simulation parameters

Parameter	Value
ULA-FDA element number	20
Subarray element number	10
Carrier frequency	10 GHz
Frequency offset	2 kHz
Array element spacing d	$c/(2f_0)$
Target location (R, θ)	(200 km, 30°)

2.2 Planar frequency diverse array

Considering the reality of radar signal processing, which requires implementation in a higher dimension than ULA-FDA, upon which existing works are mainly based, the beamforming theory for an FDA was extended to planar array geometries as proposed in Jones and Rigling (2012) with array elements in equidistant distribution in x and y axes as shown in Fig. 4.

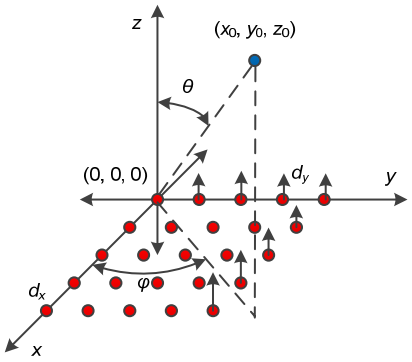

Fig. 4 Planar frequency diverse array (PFDA)

The transmitted signal corresponding to the element (n, m) in the planar frequency diverse array (PFDA) can be expressed as

$$s_{nm}(t)=\exp\left(\mathrm{j}2\pi f_{nm}t\right), \tag{8}$$

where $f_{nm}=f_0+n\Delta f_x+m\Delta f_y$, $n=0, 1, \ldots, N-1$, $m=0, 1, \ldots, M-1$. The signal arriving at the far-field target can be written as

$$s_{nm}\left(t-\frac{R_{nm}}{c}\right)=\exp\left[\mathrm{j}2\pi f_{nm}\left(t-\frac{R_{nm}}{c}\right)\right]. \tag{9}$$

Considering a far-field target (x_0, y_0, z_0), the R_0, φ_0, and θ_0 of the target can be reached. Taking the element (0, 0, 0) as the reference of the array, the

range between the reference element and the observed point is $R_0=\sqrt{x_0^2+y_0^2+z_0^2}$. Then the range between the element (n, m) and the observed far-field target can be expressed as $R_{nm}=[(x_0-x_n)^2+(y_0-y_m)^2+z_0^2]^{1/2}$. The overall signal observed at (x_0, y_0, z_0) in the far field can be written as

$$\begin{aligned}s(t;R_0,\theta_0,\varphi_0)&=\sum_{n=0}^{N-1}\sum_{m=0}^{M-1}\left\|\boldsymbol{\alpha}\left(\hat{R}_0,\hat{\theta}_0,\hat{\varphi}_0\right)\right\| s_{nm}\left(t-\frac{R_{nm}}{c}\right)\\&=\sum_{n=0}^{N-1}\sum_{m=0}^{M-1}\exp\left\{\mathrm{j}2\pi f_{nm}\left[t-\frac{R_0-\hat{R}_0}{c}\right.\right.\\&\quad+\frac{nd_x\left(\sin\theta_0\cos\varphi_0-\sin\hat{\theta}_0\cos\hat{\varphi}_0\right)}{c}\\&\quad\left.\left.+\frac{nd_y\left(\sin\theta_0\sin\varphi_0-\sin\hat{\theta}_0\sin\hat{\varphi}_0\right)}{c}\right]\right\},\end{aligned}\tag{10}$$

where $\boldsymbol{\alpha}\left(\hat{R}_0,\hat{\theta}_0,\hat{\varphi}_0\right)$ denotes the transmit steering vector. Consider that a target is located at (50, 50, 150) km, Δf_x=1 kHz, Δf_y=10 kHz, and N=M=9. Fig. 5 shows the PFDA transmit beampattern.

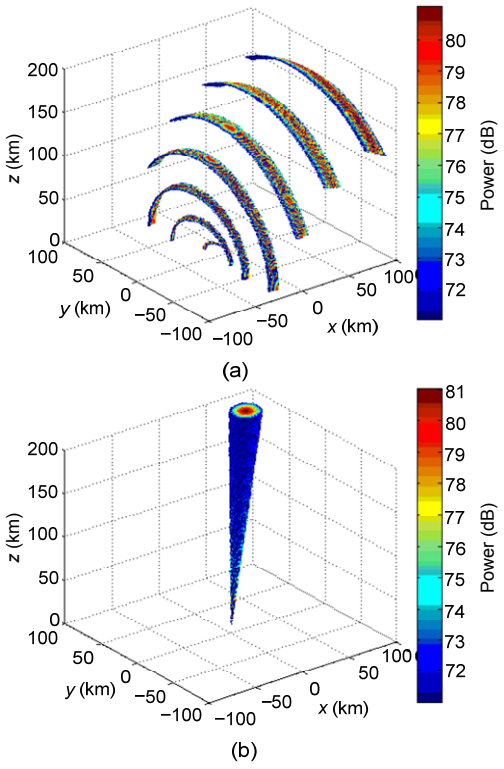

Fig. 5 Transmit beampattern based on a two-dimensional array structure: (a) PFDA transmit beampattern; (b) planar PA transmit beampattern

The regularity of the beampattern as a function of range and angle is shown in Fig. 3. This is different from that of a conventional PA, which can be easily intercepted and captured by the enemy, because the beam steering is fixed at one angle for all ranges. The FDA provides a possibility to control the transmitted energy distribution or suppress/detect range-dependent interference/targets.

3 Subarray-based FDA radar

There is range-angle coupling inherent in the transmit beampattern of the basic ULA-FDA because of the linear incremental synchronization between the element spacing and the fixed linear frequency offset. The way to eliminate the inherent range-angle coupling is the premise of accurate beam control. To eliminate the synchronization, it is suggested to adopt a specially designed FDA configuration to decouple the beampattern in the range and angle dimensions. In this section, we analyze four SB-FDA radar configurations based on ULA-FDA.

3.1 Single-sided subarray-based FDA

As shown in Fig. 6, the single-sided SB-FDA divides the basic ULA-FDA into two adjacent subarrays.

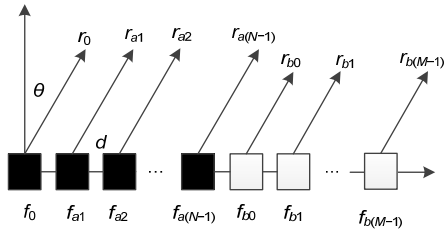

Fig. 6 Single-sided subarray-based frequency diverse array (SB-FDA)

Take the leftmost element as the reference for each subarray. Subarray a, with N antenna elements, uses the frequency offset of Δf_1. Subarray b, with M antenna elements, uses the frequency offset of Δf_2. Then the frequency radiated from the n^{th} element in subarray a and the m^{th} element in subarray b can be expressed as

$$\begin{cases}f_{an}=f_0+n\Delta f_1, & n=0,\ 1,\ \ldots,\ N-1,\\ f_{bm}=f_{b0}+m\Delta f_2, & m=0,\ 1,\ \ldots,M-1.\end{cases}\tag{11}$$

The transmit steering vector of the array can be represented by

$$\boldsymbol{\alpha}\left(\hat{R},\hat{\theta}\right)=\left[1,\ \mathrm{e}^{-\mathrm{j}\omega_a},\ \mathrm{e}^{-\mathrm{j}2\omega_a},\ \cdots,\ \mathrm{e}^{-\mathrm{j}(N-1)\omega_a},\right.$$
$$\left.1\cdot\mathrm{e}^{-\mathrm{j}\omega_c},\ \mathrm{e}^{-\mathrm{j}(\omega_c+\omega_b)},\ \mathrm{e}^{-\mathrm{j}(\omega_c+2\omega_b)},\ \cdots,\ \mathrm{e}^{-\mathrm{j}[\omega_c+(M-1)\omega_b]}\right]^{\mathrm{T}},\tag{12}$$

where

$$\begin{cases}\omega_a=\dfrac{2\pi f_0 d\sin\hat{\theta}}{c}-\dfrac{2\pi\Delta f_1\hat{R}}{c},\\ \omega_b=\dfrac{2\pi f_0 d\sin\hat{\theta}}{c}-\dfrac{2\pi\Delta f_2\hat{R}}{c},\\ \omega_c=\dfrac{2\pi N f_0 d\sin\hat{\theta}}{c}.\end{cases}$$

3.2 Centrosymmetric subarray-based FDA

Taking the central element as the reference element, the centrosymmetric SB-FDA divides the basic ULA-FDA into two subarrays that are symmetric about the reference element (Fig. 7).

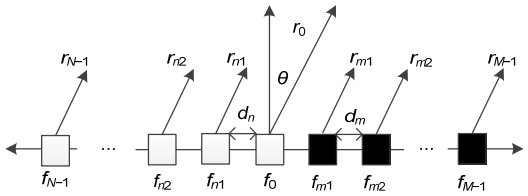

Fig. 7 Centrosymmetric subarray-based frequency diverse array (SB-FDA)

Subarray 1, with N antenna elements, uses the frequency offset of Δf_1. Subarray 2, with M antenna elements, uses the frequency offset of Δf_2. Then the frequency radiated from the n^{th} element in subarray 1 and the m^{th} element in subarray 2 can be expressed as

$$\begin{cases}f_{1n}=f_0+n\Delta f_1, & n=0,\ 1,\ \ldots,\ N-1,\\ f_{2m}=f_0+m\Delta f_2, & m=0,\ 1,\ \ldots,M-1.\end{cases}\tag{13}$$

The transmit signal of the n^{th} element in subarray 1 and the m^{th} element in subarray 2 can be written as

$$\begin{cases}s_1(t)=\exp(\mathrm{j}2\pi f_{1n}t),\ n=0,\ 1,\ \ldots,\ N-1,\\ s_2(t)=\exp(\mathrm{j}2\pi f_{2m}t),\ m=0,\ 1,\ \ldots,\ M-1.\end{cases}\tag{14}$$

The signal received by a specific far-field location (R, θ), which is transmitted by the n^{th} element in subarray 1 and the m^{th} element in subarray 2, can be written as

$$\begin{cases}s_{1n}=\exp\left[\mathrm{j}2\pi f_{1n}\left(t-\dfrac{R_n}{c}\right)\right], & n=0,\ 1,\ \cdots,\ N-1,\\ s_{2m}=\exp\left[\mathrm{j}2\pi f_{2m}\left(t-\dfrac{R_m}{c}\right)\right], & m=0,\ 1,\ \cdots,\ M-1.\end{cases}\tag{15}$$

The total electric field of subarrays 1 and 2 observed by the far-field point (R, θ) can be written as

$$\begin{cases}E_{1\mathrm{T}}=\displaystyle\sum_{n=0}^{N-1}\frac{1}{R}f_{\mathrm{e}}(\omega_0)\mathrm{e}^{\mathrm{j}(\omega_0 t-k_0R_0)}\frac{\sin\left(\dfrac{N\gamma_1}{2}\right)}{\sin\left(\dfrac{\gamma_1}{2}\right)}\mathrm{e}^{\mathrm{j}\frac{(N-1)\gamma_1}{2}},\\ E_{2\mathrm{T}}=\displaystyle\sum_{m=0}^{M-1}\frac{1}{R}f_{\mathrm{e}}(\omega_0)\mathrm{e}^{\mathrm{j}(\omega_0 t-k_0R_0)}\frac{\sin\left(\dfrac{M\gamma_2}{2}\right)}{\sin\left(\dfrac{\gamma_2}{2}\right)}\mathrm{e}^{\mathrm{j}\frac{(M-1)\gamma_2}{2}},\end{cases}\tag{16}$$

where

$$\begin{cases}\gamma_1=2\pi\left(\Delta f_1 t-\dfrac{\Delta f_1 R}{c}+\dfrac{d_1 f_0\sin\theta}{c}\right),\\ \gamma_2=2\pi\left(\Delta f_2 t-\dfrac{\Delta f_2 R}{c}+\dfrac{d_2 f_0\sin\theta}{c}\right).\end{cases}\tag{17}$$

3.3 Overlapping subarray-based FDA

Taking the leftmost element as the reference, the configuration of the overlapping SB-FDA is shown in Fig. 8.

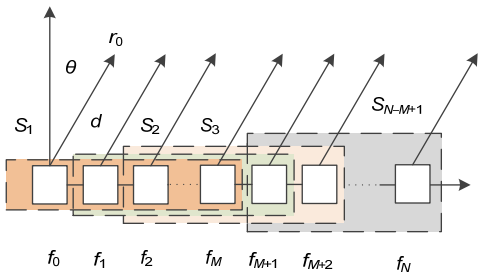

Fig. 8 Overlapping subarray-based frequency diverse array (SB-FDA)

It is observed that the basic ULA-FDA is divided into N–M+1 overlapping subarrays, denoted as $\{S_1\}$,

$\{S_2\}$, …, $\{S_{N-M+1}\}$, each of which consists of M elements. That is to say, the total element number of this array is N. The signal radiated by subarray l toward the specific far-field target (R, θ) can be expressed as

$$x_l(t,\theta,R)=\boldsymbol{w}_l^{\mathrm{H}}\boldsymbol{u}_l(\theta,R)s_l(t), \tag{18}$$

where $s_l(t)$ denotes the transmit signal of the l^{th} subarray, $\boldsymbol{w}_l$ the weight vector, and $\boldsymbol{u}_l$ the steering vector.

$$\boldsymbol{u}_l(\theta,R)=\left[\mathrm{e}^{\mathrm{j}\beta_{1,l}},\ \mathrm{e}^{\mathrm{j}\beta_{2,l}},\ \cdots,\ \mathrm{e}^{\mathrm{j}\beta_{M,l}}\right], \tag{19}$$

$$\beta_{m,l}=2\pi m\left(\frac{\Delta fR}{c}+\frac{f_0 d\sin\theta}{c}\right). \tag{20}$$

3.4 Cross subarray-based FDA

Take all the odd array elements of the basic ULA-FDA to make up subarray a and all the even array elements to form subarray b. Then the basic ULA-FDA is divided into the cross SB-FDA (Fig. 9).

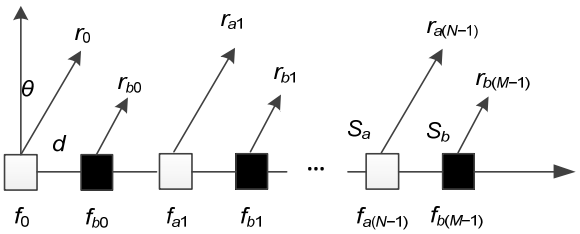

Fig. 9 Cross subarray-based frequency diverse array (SB-FDA)

Under narrowband conditions, the signal arriving at the far-field observation point (R, θ), which is transmitted by the n^{th} element of subarray a and the m^{th} element of subarray b, can be written as

$$s_{an}=\exp\left[\mathrm{j}2\pi(f_0+n2\Delta f)\left(t-\frac{R_0-nd\sin\theta}{c}\right)\right], \tag{21}$$

$$s_{bm}=\exp\left[\mathrm{j}2\pi\left(f_0+\Delta f+m2\Delta f\right)\left(t-\frac{R_0-md\sin\theta}{c}\right)\right], \tag{22}$$

where Δf represents the frequency offset, d is the element spacing, and N and M represent the number of array elements of subarrays a and b, respectively.

4 Subarray-based dot-shaped beamforming

4.1 Nonlinear frequency offset

To decouple the FDA range-angle-dependent beampattern, the best way is to form a dot-shaped beampattern without periodicity in the maximum rather than the trailing beampattern of log-FDA. This can be achieved by the array configuration design as well as the frequency offset design. The beampattern decoupling method based on nonlinear frequency offset is the premise for suppressing range-related interference. In this subsection, we analyze the range-angle joint estimation performance of the FDA using four different nonlinear frequency offsets.

Considering L targets located in the space, the FDA array received signal obtained by the matched filtering can be given as

$$\boldsymbol{x}(\theta,r,\tau)=\sum_{l=1}^{L}\boldsymbol{\alpha}_l(\theta,r,\tau)\boldsymbol{w}_u^{\mathrm{H}}\boldsymbol{a}(\theta,r,\tau)+\boldsymbol{n}(\theta,r,\tau), \tag{23}$$

where $\boldsymbol{\alpha}_l$ denotes the target reflection coefficient, $\boldsymbol{n}$ the Gaussian white noise, $\boldsymbol{a}$ the steering vector, and $\boldsymbol{w}_u=\boldsymbol{a}$ the reception weight vector.

When the target position is determined, the delay τ can be formulated by the target azimuth θ and the slant range r. Eq. (23) can be rewritten as

$$\boldsymbol{x}(\theta,r)=\sum_{l=1}^{L}\boldsymbol{\alpha}_l(\theta,r)\boldsymbol{w}_u^{\mathrm{H}}\boldsymbol{a}(\theta,r)+\boldsymbol{n}(\theta,r), \tag{24}$$

where

$$\begin{cases}\boldsymbol{a}(\theta,r)=\left[1,\ \mathrm{e}^{\mathrm{j}\phi_1},\ \cdots,\ \mathrm{e}^{\mathrm{j}\phi_n},\ \cdots,\ \mathrm{e}^{\mathrm{j}\phi_{N-1}}\right],\\ \phi_n=2\pi\left(\dfrac{f_0 nd\sin\theta}{c}-\dfrac{\Delta f_n r}{c}+\dfrac{n\Delta f_n d\sin\theta}{c}\right).\end{cases}$$

The received signal covariance matrix is expressed as

$$\boldsymbol{R}_x=E\left\{\boldsymbol{x}(\theta,r)\boldsymbol{x}^{\mathrm{H}}(\theta,r)\right\}=\boldsymbol{U}\cdot E\left\{\boldsymbol{\alpha}\boldsymbol{\alpha}^{\mathrm{H}}\right\}\boldsymbol{U}^{\mathrm{H}}+\sigma_n^2\boldsymbol{I}, \tag{25}$$

where σ_n^2 is the noise mean square error, $\boldsymbol{I}$ denotes the unit matrix, and $\boldsymbol{U}=[\boldsymbol{a}(\theta_1, r_1), \boldsymbol{a}(\theta_2, r_2), \ldots, \boldsymbol{a}(\theta_L, r_L)]$.

Then the eigenvalue decomposition of the covariance matrix is performed. The eigenvalues are rearranged according to their values. The eigenvectors corresponding to the eigenvalues are regarded as the signal subspace. The remaining eigenvectors are regarded as the noise subspace. Finally, we calculate the peak of the spectral function by

$$P(\theta,r)=\frac{1}{\boldsymbol{a}_r^{\mathrm{H}}(\theta,t)\boldsymbol{U}_n\boldsymbol{U}_n^{\mathrm{H}}\boldsymbol{a}_r(\theta,t)}, \tag{26}$$

where $\boldsymbol{a}_r(\theta, t)$ denotes the steering vector and $\boldsymbol{U}_n$ the signal subspace.

Consider a far-field target located at (0°, 500 km). Fig. 10 shows the multiple signal classification (MUSIC) spectrum of the basic ULA-FDA with logarithmic, sinusoidal, cubic, and reciprocal frequency offsets. The FDA with sinusoidally increasing frequency offset, called sin-FDA, has remarkable performance advantages. Therefore, we introduce a sinusoidally increasing frequency offset into SB-FDA.

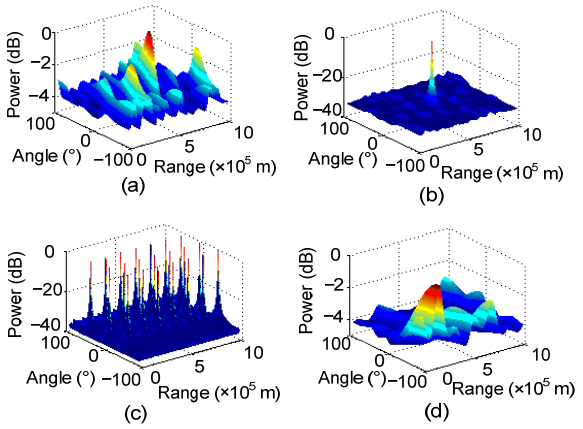

Fig. 10 MUSIC spectrum when θ=0° and R_0=500 km: (a) log-FDA; (b) sin-FDA; (c) cubic-FDA; (d) reciprocal-FDA

Signals transmitted by the n^{th} element of sin-FDA can be expressed as

$$s_{tn}(t,\theta,R)=\exp\left\{\mathrm{j}2\pi\left[f_0+\sin(n)\Delta f\right]\left(t-\frac{r_n}{c}\right)\right\}. \tag{27}$$

We can control the maximum of the transmit beam to the desired target location $\left(\hat{R}_0,\hat{\theta}_0\right)$ by optimizing the complex weight $\alpha_n\left(\hat{R}_0,\hat{\theta}_0\right)$, expressed as

$$\alpha_n(\hat{R}_0,\hat{\theta}_0)=\exp\left\{-\mathrm{j}2\pi\left[\frac{f_0\hat{R}_0}{c}-\frac{f_0nd\sin\hat{\theta}_0}{c}+\frac{\sin(n)\Delta f\hat{R}_0}{c}-\frac{\sin(n)\Delta fnd\sin\hat{\theta}_0}{c}\right]\right\}. \tag{28}$$

The signal arriving at the target is expressed as

$$s_{tn}\left(t,\hat{R}_0,\hat{\theta}_0\right)=\alpha_n^{\mathrm{H}}\left(\hat{R}_0,\hat{\theta}_0\right)s_{tn}(t,\theta,R), \tag{29}$$

where $[\cdot]^{\mathrm{H}}$ denotes the conjugate operator.

4.2 Elements transmitting at multiple frequencies

The basic ULA-FDA radar transmits an identical baseband waveform at each element with a coherent single frequency. In this study, we use multi-carrier frequencies on each element of the four analyzed subarray-based sin-FDAs to decouple the transmit beampattern.

The signal of the n^{th} element of sin-FDA simultaneously transmitting the l^{th} frequency component can be written as

$$x_{nl}(t)=w_{nl}\exp\left[\mathrm{j}2\pi f_{nl}\left(t-\frac{r_n}{c}\right)\right], \tag{30}$$

where $f_{nl}=f_0+\Delta f_n+\Delta f_l$ denotes the radiation frequency of the n^{th} element and the l^{th} frequency component, $\Delta f_n=\sin(n)\Delta f$ (n=0, 1, …, N−1) is the frequency offset between the n^{th} element and the reference element, N is the array number for the given array aperture, $\Delta f_l=\sin(l)\Delta f$ (l=0, 1, …, L−1) represents the frequency offset of each array element transmitting the l^{th} frequency component, and L is the total number of frequency components transmitted by each array element.

The total signal received by the far-field observation target can be expressed as

$$\begin{aligned}x_{nl}(t,R,\theta)&=\sum_{n=0}^{N-1}\sum_{l=0}^{L}x_{nl}(t)\\&=\sum_{n=0}^{N-1}\sum_{l=0}^{L}w_{nl}\exp\left[\mathrm{j}2\pi f_{nl}\left(t-\frac{r_n}{c}\right)\right]\\&=\sum_{n=0}^{N-1}\sum_{l=0}^{L}w_{nl}\left\{\mathrm{j}2\pi\left[f_0+\Delta f\left(\sin n+\sin l\right)\right]\cdot\left(t-\frac{R-nd\sin\theta}{c}\right)\right\},\end{aligned} \tag{31}$$

where w_{nl} is the transmit weight for each array element, and (R, θ) is an arbitrary far-field observation point. The transmit beampattern of sin-FDA transmitting multiple frequencies can be expressed as

$$B(t,R,\theta)=\left|\sum_{n=0}^{N-1}\sum_{l=0}^{L}w_{nl}\exp\left(\frac{f_0 nd\sin\theta}{c}\right)\cdot\exp\left(\mathrm{j}2\pi\Delta f(\sin n+\sin l)\left(t-\frac{R}{c}\right)\right)\right|^2. \quad (32)$$

5 Dot-shaped beamforming of subarray-based PFDA

Most existing works on dot-shaped beamforming focus only on ULA-FDA. In practice, radar applications require the ability to beam steer in high dimensions, which will exceed the capability of the one-dimensional uniform linear array. In this section, we divide the basic PFDA proposed in Jones and Rigling (2012) into three subarray-based PFDAs (Fig. 11).

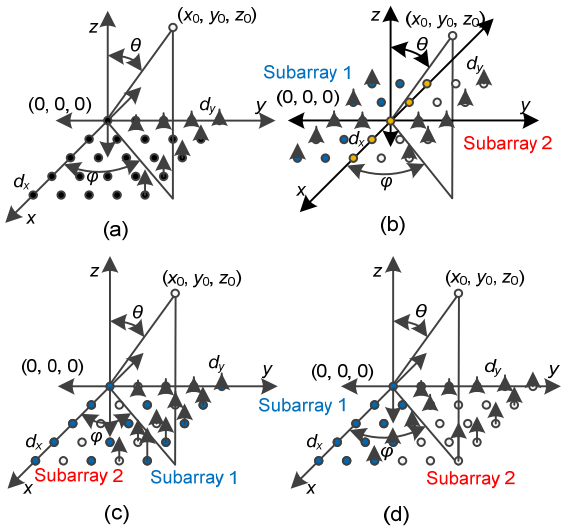

Fig. 11 Four subarray-based PFDAs: (a) basic PFDA; (b) symmetric subarray-based PFDA; (c) single-sided PFDA; (d) cross PFDA

The dot-shaped beam can be achieved by employing both positive and negative nonlinear frequency offsets proposed in Jones and Rigling (2012) between the array elements in the x and y axes of the subarray-based sin-log-PFDA. The carrier frequency of the antenna element (n, m) is $f_{nm}=f_0+\sin(n)\Delta f_x+\log(m+1)\Delta f_y$, where $f_0=10$ GHz. The offset frequencies of subarray 1 are $\Delta f_x=1$ kHz and $\Delta f_y=10$ kHz, and the offset frequencies of subarray 2 are $\Delta f_x=-1$ kHz, $\Delta f_y=-10$ kHz, $\Delta f_{nx}=\sin(n)\Delta f_x$, and $\Delta f_{my}=\log(m+1)\Delta f_y$. The far-field target locates at (50, 50, 150) km. The transmit beampatterns of the three proposed subarray-based PFDAs (SB-PFDAs) and the basic PFDA are presented in the next section.

6 Simulation and results

In this section, simulation is performed to verify the effectiveness of the proposed approach. We assume a basic ULA-FDA of 20 sensors spaced a half-wavelength apart. The rest of the parameters are listed in Table 1.

Example 1 Transmit beampattern of the four SB-FDAs with a fixed frequency offset

The transmit beampattern of the four SB-FDAs analyzed above can be physically explained as a joint interferometry effect caused by different amplitude responses of the subarrays in the target position. Figs. 12–16 show the transmit beampattern of the centrosymmetric SB-FDA, the single-sided SB-FDA, the overlapping SB-FDA, the cross SB-FDA, and the log-FDA, respectively.

Fig. 12 shows that, unlike the coupled S-shaped range-angle beampattern of ULA-FDA, the centrosymmetric SB-FDA can form a dot-shaped beam at the target position. Fig. 13 shows that the beampattern of the single-sided SB-FDA is not significantly different from that of the basic ULA-FDA. There exists a mainlobe distortion at the target position. Figs. 14 and 15 show that the overlapping SB-FDA and the cross SB-FDA both form a trailing beam in the scanning position, which has a certain effect on eliminating the inherent range-angle coupling. However, it is similar to the decoupling method with logarithmically increasing frequency offset shown in Fig. 16, which achieves poor resolution in both the range and angle dimensions. Comparing the beam width of the four SB-FDAs in both angle and range dimensions, it is obvious that the overlapping SB-FDA has the highest precision. However, the realization of the overlapping SB-FDA is difficult in a physical implementation. Considering the frequency changes across the array

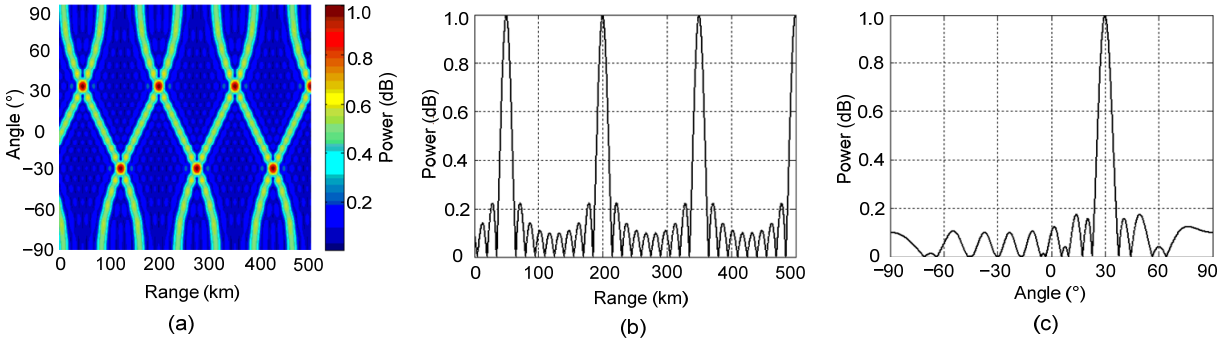

Fig. 12 Centrosymmetric SB-FDA transmit beampattern: (a) range and angle dimensions; (b) range dimension at the target position; (c) angle dimension at the target position

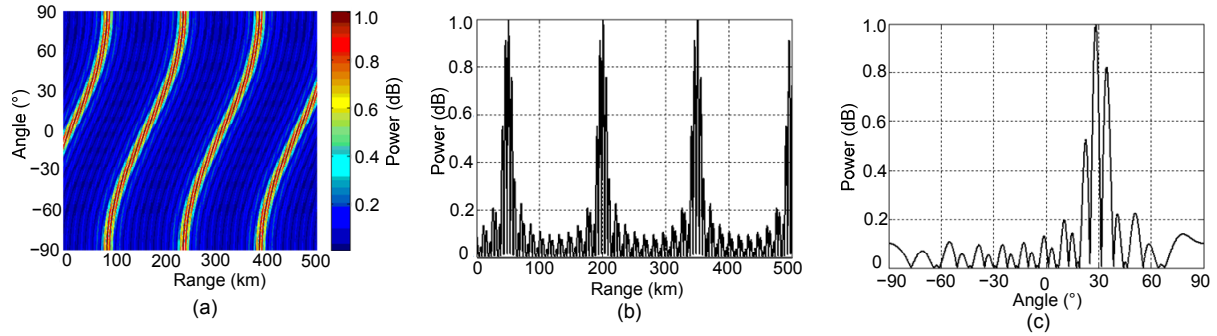

Fig. 13 Single-sided SB-FDA transmit beampattern: (a) range and angle dimensions; (b) range dimension at the target position; (c) angle dimension at the target position

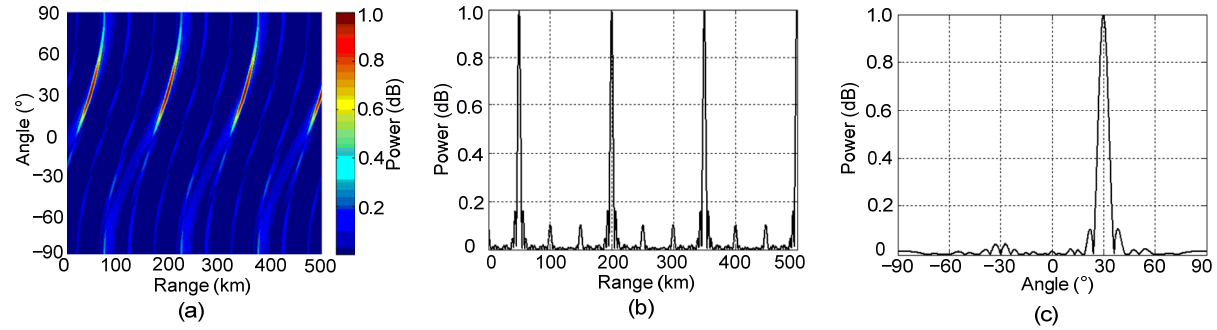

Fig. 14 Overlapping SB-FDA transmit beampattern: (a) range and angle dimensions; (b) range dimension at the target position; (c) angle dimension at the target position

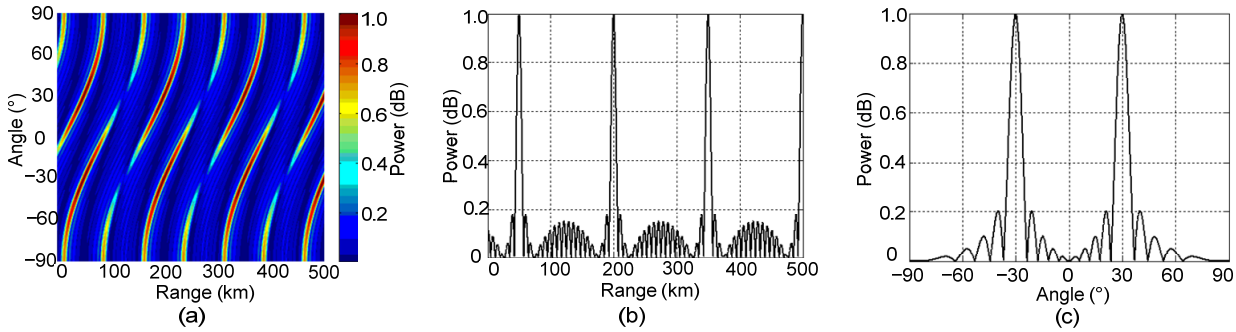

Fig. 15 Cross SB-FDA transmit beampattern: (a) range and angle dimensions; (b) range dimension at the target position; (c) angle dimension at the target position

elements, the design of the transmitter and receiver will be difficult. Considering the multiple maxima at different ranges in the beampattern of SB-FDAs, which are easily disturbed, the decoupling method based on the array configuration design requires further optimization to remove the periodicity in the maximum.

Example 2 Transmit beampattern of the four SB-FDAs with a sinusoidal frequency offset

It can be seen from Fig. 17 that the transmit beampatterns of the single-sided SB-FDA, centrosymmetric SB-FDA, overlapping SB-FDA, and cross SB-FDAs are all range-angle decoupled by forming a dot-shaped beam in the target position: (1) Considering the overlay airspace of the mainlobe, $S_b>S_d>S_c>S_a$; (2) Considering the sidelobe's magnitude, the performance of the overlapping SB-FDA is the most ideal; (3) Considering the shape of the beampattern, all the four SB-FDAs can form a dot-shaped beam in the target position. The performances of the overlapping SB-FDA and the centrosymmetric SB-FDA are relatively ideal. Considering that the dot-shaped beam of the single-sided SB-FDA is accompanied by high sidelobes and that the image

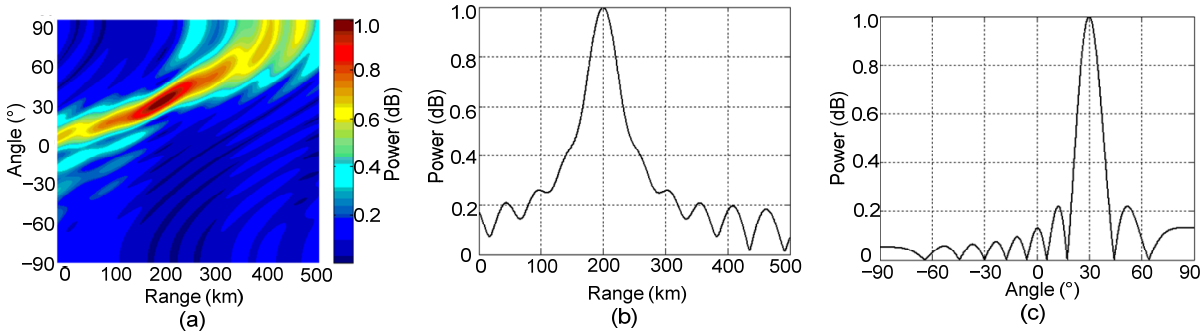

Fig. 16 Log-FDA transmit beampattern: (a) range and angle dimensions; (b) range dimension at the target position; (c) angle dimension at the target position

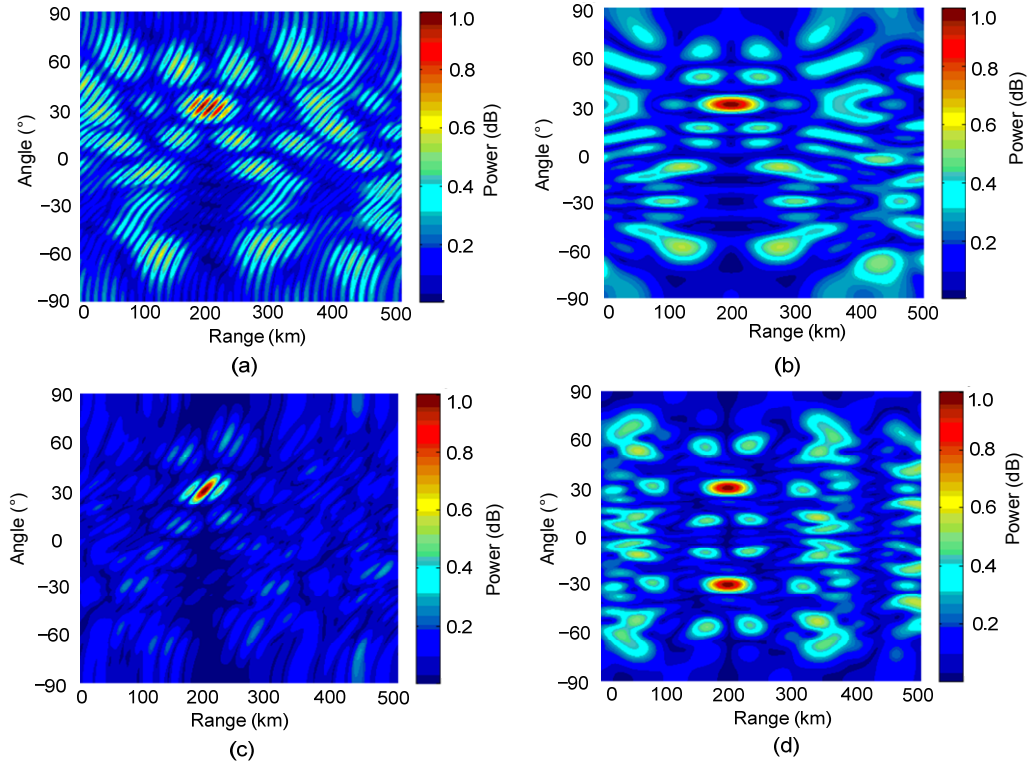

Fig. 17 Transmit beampattern of the four subarray-based sin-FDAs: (a) single-sided SB-FDA; (b) centrosymmetric SB-FDA; (c) overlapping SB-FDA; (d) cross SB-FDA

mainlobe beam exists in the beampattern of the cross SB-FDA, the sidelobes requires further optimization.

Example 3 Transmit beampattern based on four subarray-based sin-FDAs transmitting multiple frequencies

On the basis of Example 2, further analysis concerning the transmit beampatterns of the single-sided SB-FDA, centrosymmetric SB-FDA, overlapping SB-FDA, and cross SB-FDA transmitting multiple frequencies is presented in Fig. 18. In Example 3, the total number of frequency components transmitted by each array element is 3. The frequency offset is shown in Table 1. It can be seen that there is only one single maximum at the target location, which can focus the transmit energy in a desired spatial region: (1) Considering the overlay airspace of the target position, S_b>S_d>S_c>S_a; (2) Considering the mainbeam peak-to-sidelobe ratio, the performance of the overlapping SB-FDA is the most ideal; (3) Considering the beam shape, apart from the single-sided SB-FDA without remarkable improvement, the other three SB-FDAs can all form a dot-shaped beam at the target position. The sidelobe disturbances of the cross SB-FDA, overlapping SB-FDA, and centrosymmetric SB-FDA are reduced. The peaks lying in the image position formed by the cross SB-FDA are removed. The essence of SB-FDA is to divide the basic ULA-FDA into multiple subarrays, employing the same or distinct frequency increments. As a result, the target's range and angle based on the proposed method will be directly estimated from the transmit-receiver beamforming output peak with high accuracy.

Example 4 Comparison of the angle and range dimensional beampatterns

We examine the resolution in the range and angle dimensions of log-FDA and compare the four subarray-based sin-FDAs transmitting multiple frequencies in Fig. 19. The beampattern of log-FDA has wide spread in the maxima, which may result in an ambiguous tracking performance. Figs. 19a–19e show that the beamwidth in the angle of the four subarray-based sin-FDAs transmitting multiple frequencies is between 10° and 20°, while that of the log-FDA is several times that of the four SB-FDAs. Figs. 19f–19j show that the beamwidth of the four subarray-based sin-FDAs is much smaller than that of

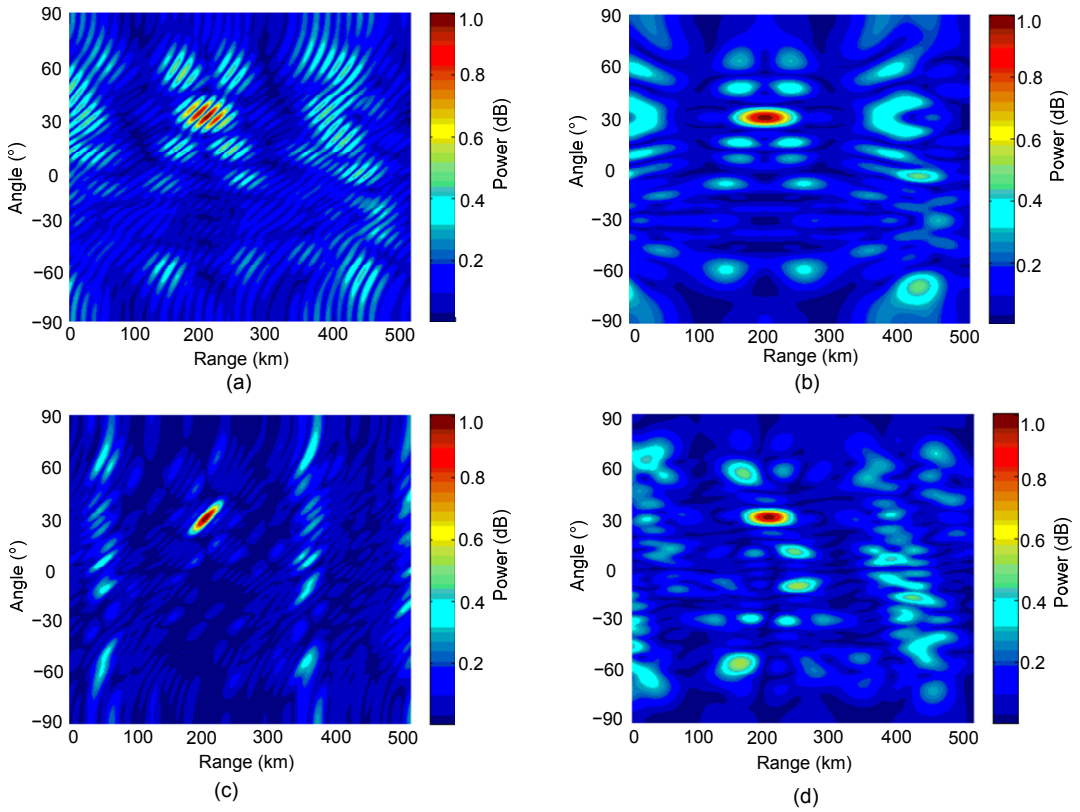

Fig. 18 Transmit beampattern of the four subarray-based sin-FDAs transmitting multiple frequencies: (a) single-sided SB-FDA; (b) centrosymmetric SB-FDA; (c) overlapping SB-FDA; (d) cross SB-FDA

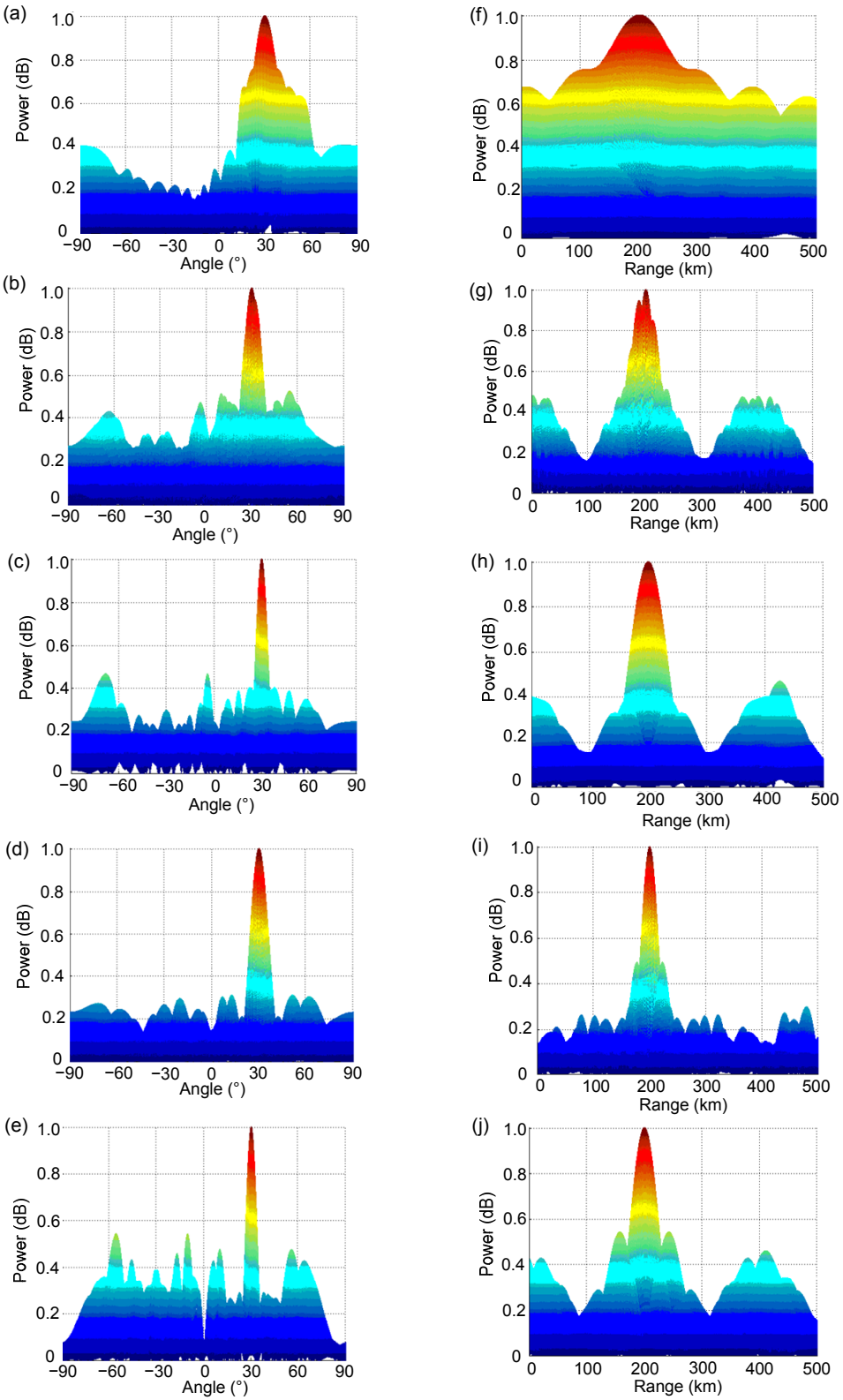

Fig. 19 Comparison of angle and range dimensional beampatterns

(a)–(e) angle and power dimensions of log-FDA, single-sided SB-FDA, centrosymmetric SB-FDA, overlapping SB-FDA, and cross SB-FDA, respectively; (f)–(j) range and power dimensions of log-FDA, single-sided SB-FDA, centrosymmetric SB-FDA, overlapping SB-FDA, and cross SB-FDA, respectively

log-FDA. We can conclude that the proposed SB-FDA scheme can produce narrow dot-shaped beam steering to the target. With the same total frequency offset, the centrosymmetric SB-FDA and the cross SB-FDA have better decoupling performance in both angle and range dimensions. It can be seen in Fig. 20 that the signal-to-interference-plus-noise ratio (SINR) of the proposed SB-FDA is better than that of log-FDA. Thus, the proposed system has better robustness against interference. Fig. 21 shows the detection probability versus the signal-noise ratio (SNR) for the proposed SB-FDA and log-FDA. The proposed FDA exhibits better detection performance compared with log-FDA. The improvement in performance in terms of SINR and the detection probability can be attributed to the sinusoidal offset across the transmit array.

Example 5 Dot-shaped beamforming for SB-FDA with different array elements

In Example 5, we take the centrosymmetric SB-FDA transmitting multiple frequencies as an example to analyze the influence of parameters, such as the number of array elements, the frequency offset, and the total number of frequency components transmitted by each array element on the performance of the transmit beampattern. Fig. 22 shows the transmit beampattern when N=10, Δf=1 kHz, and L=3. Fig. 23 shows the transmit beampattern when N=30, Δf=3 kHz, and L=3. Fig. 24 shows the transmit beampattern when N=20, Δf=2 kHz, and L=5. Based on the comprehensive analysis of Figs. 22–24, the proposed method can form a dot-shaped beam with low sidelobes and much concentrated mainlobe energy at the target position. As the number of array elements increases, the frequency offset increases and the total number of frequency components transmitted by each array element also increases.

Example 6 Dot-shaped beamforming for the subarray-based PFDA

Fig. 25a shows the 10-dB beamwidth of the mainbeam of the basic PFDA with carrier frequency of $f_{nm}=f_0+\log(n+1)\Delta f_x+\log(m+1)\Delta f_y$ and $\Delta f_x=\Delta f_y=$ 2 kHz. Figs. 25c–25d show the 10-dB beamwidth of the mainbeam of the three subarray-based PFDAs with carrier frequency $f_{nm}=f_0+\sin(n)\Delta f_x+\log(m+1)\Delta f_y$. It can be seen from Fig. 25 that the transmit beampattern of the three subarray-based PFDAs can form a dot-shaped beam in the target position:

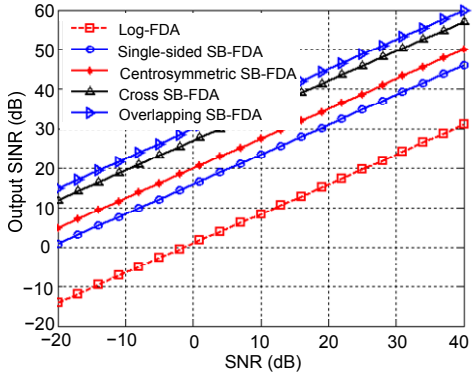

Fig. 20 Performance comparison of the SINR of different FDA radars

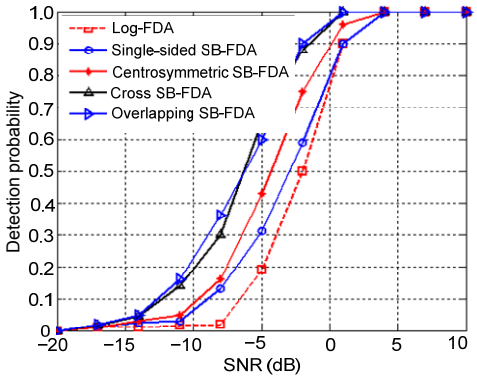

Fig. 21 Detection probability versus SNR

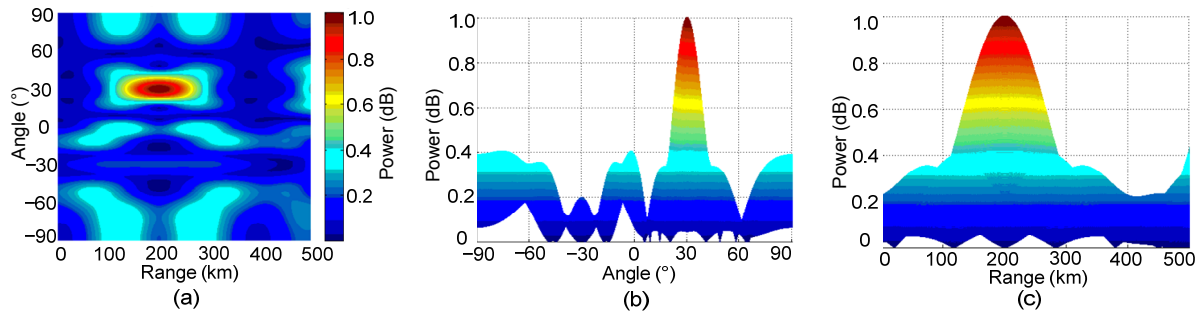

Fig. 22 Transmit beampattern of the centrosymmetric SB-FDA when N=10, Δf=1 kHz, and L=3: (a) top view; (b) left view; (c) front view

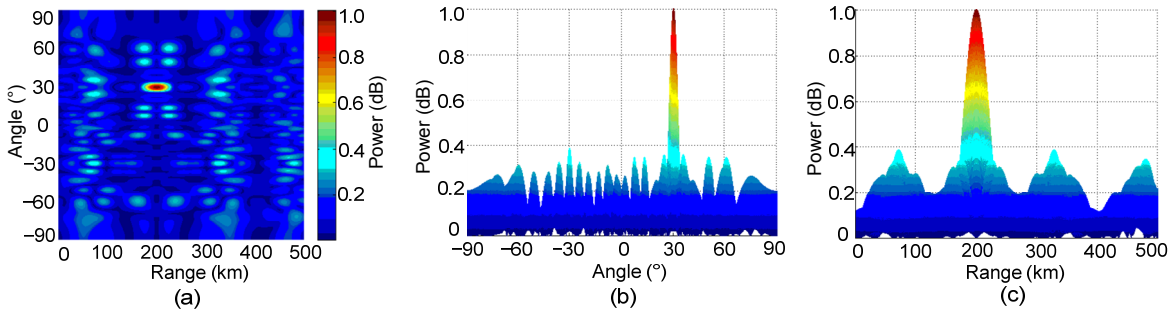

Fig. 23 Transmit beampattern of the centrosymmetric SB-FDA when N=30, Δf=3 kHz, and L=3: (a) top view; (b) left view; (c) front view

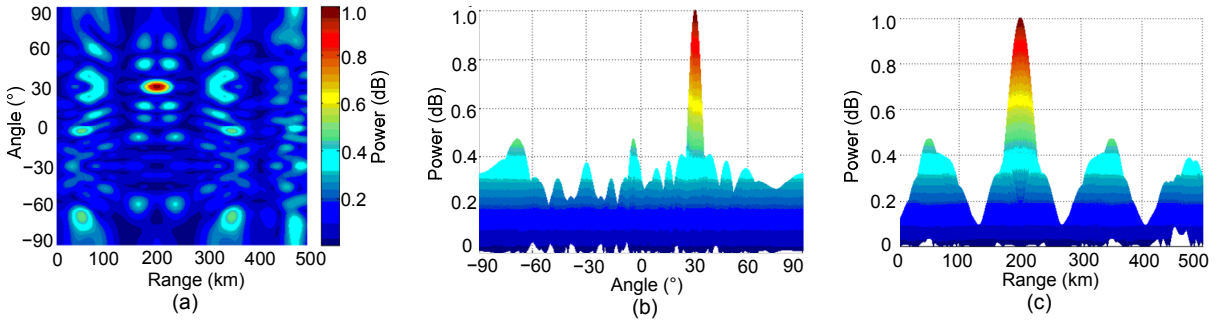

Fig. 24 Transmit beampattern of the centrosymmetric SB-FDA when N=20, Δf=2 kHz, and L=5: (a) top view; (b) left view; (c) front view

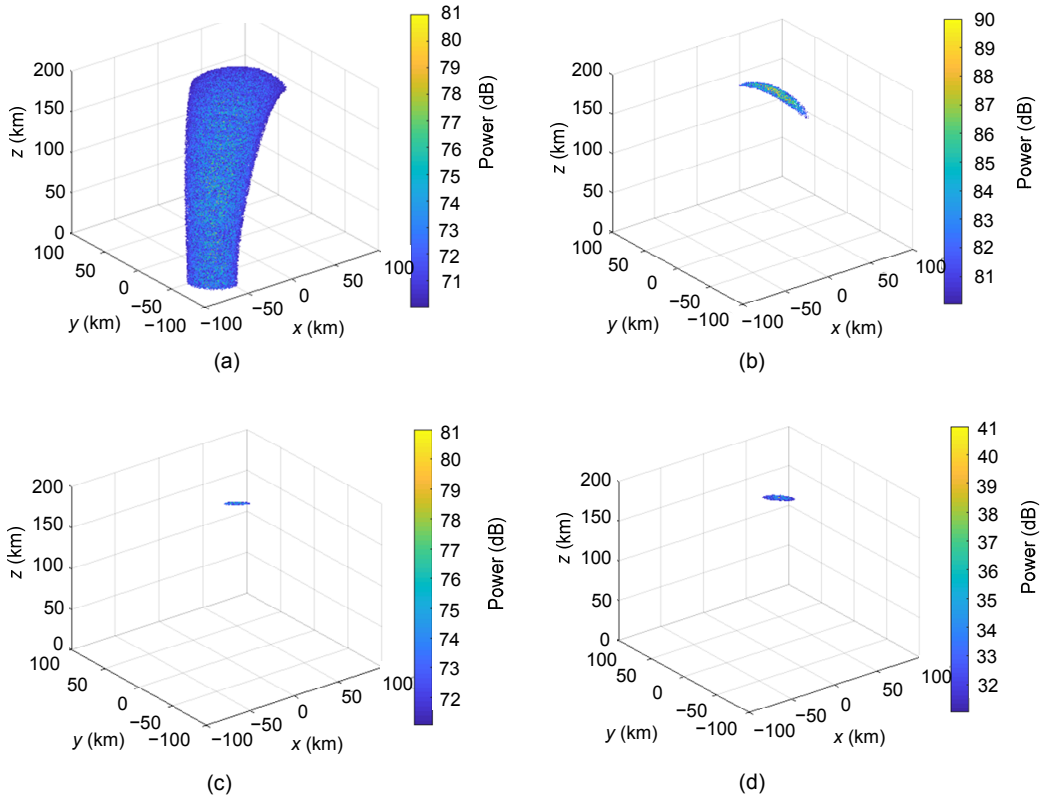

Fig. 25 Transmit beampattern of the PFDA: (a) basic PFDA with a logarithmic offset; (b) symmetric SB-PFDA; (c) single-sided SB-PFDA; (d) cross SB-PFDA

(1) Considering the overlay airspace of the mainlobe, $a>b>d>c$; (2) Considering the sidelobe magnitude, the single-sided subarray-based PFDA is the most ideal; (3) Considering the directional gain, $b>c=a>d$. The symmetric SB-PFDA beam pointing has the highest directional gain at the target location. It can be seen in Fig. 26 that the SINR of the symmetric SB-PFDA is better than that of the other three PFDA arrays. The conclusion can be used to suppress the range-related interference.

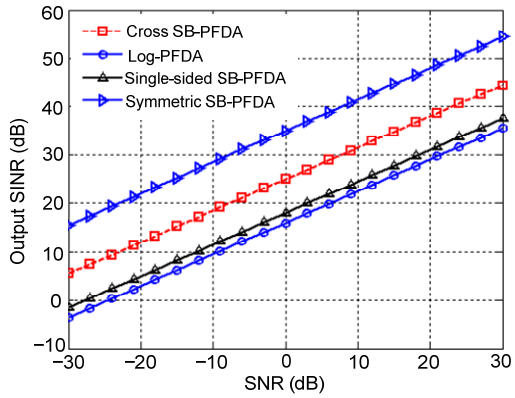

Fig. 26 SINR versus SNR performance

7 Conclusions

FDA radar has received increasing attention in recent years because of the controllable degrees of freedom. In this study, a dot-shaped beam based on SB-FDA is realized. Comparisons of the proposed subarray-based sin-FDA transmitting multiple frequencies with log-FDA in simulations showed improvement in the transmit beampatterns. The subarray-based structure simplified the processing and assembly of the array, providing a wide signal bandwidth. It has wide application potential in the fields of range-angle joint estimation, front-view detection, and imaging of radar targets. Furthermore, research will be carried out based on the time-invariant SB-FDA.

Compliance with ethics guidelines

Bo WANG, Jun-wei XIE, Jing ZHANG, and Jia-ang GE declare that they have no conflict of interest.

References

Antonik P, Wicks MC, Griffiths HD, et al., 2006a. Frequency diverse array radars. Proc IEEE Conf on Radar, p.215-217. https://doi.org/10.1109/RADAR.2006.1631800

Antonik P, Wicks MC, Griffiths HD, et al., 2006b. Range-dependent beamforming using element level waveform diversity. Proc Int Waveform Diversity and Design Conf, p.71-76. https://doi.org/10.1109/WDD.2006.8321488

Baizert P, Hale TB, Temple MA, et al., 2006. Forward-looking radar GMTI benefits using a linear frequency diverse array. *Electron Lett*, 42(22):1311-1312. https://doi.org/10.1049/el:20062791

Basit A, Qureshi IM, Khan W, et al., 2015. Cognitive frequency offset calculation for frequency diverse array radar. Proc 12th Int Bhurban Conf on Applied Sciences and Technology, p.641-645. https://doi.org/10.1109/IBCAST.2015.7058575

Basit A, Qureshi IM, Khan W, et al., 2017. Beam pattern synthesis for an FDA radar with hamming window-based nonuniform frequency offset. *IEEE Antenn Wirel Propag Lett*, 16:2283-2286. https://doi.org/10.1109/LAWP.2017.2714761

Cetintepe C, Demir S, 2014. Multipath characteristics of frequency diverse arrays over a ground plane. *IEEE Trans Antenn Propag*, 62(7):3567-3574. https://doi.org/10.1109/TAP.2014.2316292

Fenn AJ, 2008. Adaptive Antennas and Phased Arrays for Radar and Communications. Artech House, Norwood, MA, USA.

Hansen RC, 2009. Phased Array Antennas (2nd Ed.). John Wiley & Sons, New Jersey, USA. https://doi.org/10.1002/9780470529188

Hu JS, Yan SH, Shu F, et al., 2017. Artificial-noise-aided secure transmission with directional modulation based on random frequency diverse arrays. *IEEE Access*, 5:1658-1667. https://doi.org/10.1109/ACCESS.2017.2653182

Jones AM, Rigling BD, 2012. Planar frequency diverse array receiver architecture. Proc Radar Conf, p.145-150. https://doi.org/10.1109/RADAR.2012.6212127

Keizer WPMN, 2011. Low sidelobe phased array pattern synthesis with compensation for errors due to quantized tapering. *IEEE Trans Antenn Propag*, 59(12):4520-4524. https://doi.org/10.1109/TAP.2011.2165509

Khan W, Qureshi IM, Saeed S, 2014. Frequency diverse array radar with logarithmically increasing frequency offset. *IEEE Antenn Wirel Propag Lett*, 14:499-502. https://doi.org/10.1109/LAWP.2014.2368977

Khan W, Qureshi IM, Basit A, et al., 2015. Range-bins-based MIMO frequency diverse array radar with logarithmic frequency offset. *IEEE Antenn Wirel Propag Lett*, 15:885-888. https://doi.org/10.1109/LAWP.2015.2478964

Khan W, Qureshi IM, Basit A, et al., 2016a. Performance analysis of MIMO-frequency diverse array radar with variable logarithmic offsets. *Prog Electromagn Res C*, 62:23-34. https://doi.org/10.2528/PIERC16010902

Khan W, Qureshi IM, Basit A, et al., 2016b. Transmit/received beamforming for MIMO log-frequency diverse array

radar. Proc 13th Int Bhurban Conf on Applied Sciences and Technology, p.689-693. https://doi.org/10.1109/IBCAST.2016.7429955

Li Q, Huang L, So HC, et al., 2017. Beampattern synthesis for frequency diverse array via reweighted ℓ_1 iterative phase compensation. *IEEE Trans Aerosp Electron Syst*, 54(1): 467-475. https://doi.org/10.1109/TAES.2017.2735638

Liu YM, 2016. Range azimuth indication using a random frequency diverse array. Proc IEEE Int Conf on Acoustics, Speech and Signal Processing, p.3111-3115. https://doi.org/10.1109/ICASSP.2016.7472250

Sammartino PF, Baker CJ, Griffiths HD, 2013. Frequency diverse MIMO techniques for radar. *IEEE Trans Aerosp Electron Syst*, 49(1):201-222. https://doi.org/10.1109/TAES.2013.6404099

Shao H, Dai H, Xiong H, et al., 2016. Dot-shaped range-angle beampattern synthesis for frequency diverse array. *IEEE Antenn Wirel Propag Lett*, 15:1703-1706. https://doi.org/10.1109/LAWP.2016.2527818

Shin J, Choi JH, Kim J, et al., 2013. Full-wave simulation of frequency diverse array antenna using the FDTD method. Proc Conf on Asia-Pacific Microwave, p.1070-1072. https://doi.org/10.1109/APMC.2013.6695023

Wang SL, Xu ZH, Liu XH, et al, 2018. A novel transmit-receive system of frequency diverse array radar for multitarget localization. *Electronics*, 7(12), Article 408. https://doi.org/10.3390/electronics7120408

Wang WQ, 2014. Subarray-based frequency diverse array radar for target range-angle estimation. *IEEE Trans Aerosp Electron Syst*, 50(4):3057-3067. https://doi.org/10.1109/TAES.2014.120804

Wang WQ, So HC, 2014. Transmit subaperturing for range and angle estimation in frequency diverse array radar. *IEEE Trans Signal Process*, 62(8):2000-2011. https://doi.org/10.1109/TSP.2014.2305638

Wang WQ, Shao HZ, Cai JY, 2012. Range-angle-dependent beamforming by frequency diverse array antenna. *Int J Antenn Propag*, 2012:760489. https://doi.org/10.1155/2012/760489

Wang WQ, So HC, Shao HZ, 2014. Nonuniform frequency diverse array for range-angle imaging of targets. *IEEE Sens J*, 14(8):2469-2476. https://doi.org/10.1109/JSEN.2014.2304720

Wang YX, Huang GC, Li W, 2016. Transmit beampattern design in range and angle domains for MIMO frequency diverse array radar. *IEEE Antenn Wirel Propag Lett*, 16:1003-1006. https://doi.org/10.1109/LAWP.2016.2616193

Wicks MC, Antonik P, 2008. Frequency Diverse Array with Independent Modulation of Frequency, Amplitude, and Phase. US Patent 731 942 7B2.

Wicks MC, Antonik P, 2009. Method and Apparatus for a Frequency Diverse Array. US Patent 2 009 001 547 4A1.

Xu YH, Shi XW, Xu JW, et al., 2015. Range-angle-dependent beamforming of pulsed frequency diverse array. *IEEE Trans Antenn Propag*, 63(7):3262-3267. https://doi.org/10.1109/TAP.2015.2423698

Xu YH, Shi XW, Xu JW, et al., 2017. Range-angle-decoupled beampattern synthesis with subarray-based frequency diverse array. *Dig Signal Proc*, 64:49-59. https://doi.org/10.1016/j.dsp.2017.02.005

Zhang ZJ, Xie JW, Sheng C, et al., 2017. Deceptive jamming discrimination based on range-angle localization of frequency diverse array. *Front Inform Technol Electron Eng*, 18(9):1437-1447. https://doi.org/10.1631/FITEE.1601577